Natural convection and entropy generation of ultrafine atmospheric aerosols in the presence of hydrodynamic partial slip and thermal radiation due to solar energy

O. Ghaffarpasand*

Department of Physics, University of Isfahan, Isfahan 81746, Iran.

Abstract. Combined effects of hydrodynamic partial slip, thermal radiation due to solar energy, and nanoparticles volume fraction on natural convection and entropy generation of atmospheric ultrafine aerosols sample enclosed within a two-sided lid-driven cavity are studied numerically in the present contribution. Partial slip effect is taken into account along the two horizontal moving walls, and thermal radiation is considered through Rosseland approximation. The governing equations are solved using an accurate finite volume method based on SIMPLE algorithm. The impact of Brownian motion of nanoparticles is also considered in this study, whereby KKL (Koo-Kleinstreuer-Li) correlation is utilized for simulating the effective thermal conductivity and viscosity of nanofluid. The heatline visualization technique is also utilized to study the energy flux within the cavity. A comprehensive study is conducted on the controlling parameters, including partial slip coefficient ($\lambda = 0 - 5$), radiation parameter ($Rd = 0 - 2$), and nanoparticles volume fraction ($\phi = 0 - 4\%$), which influence the flow and heat transfer characteristics. Results show that the partial slip usually eliminates the effect of mechanical forces provoked by the moving lids. Moreover, thermal radiation homogenizes the medium thermally, which results in decreasing the average entropy generation. It is also observed that the effect of carbon-black nanoparticles on the atmospheric heat transfer manifests a wide variety of fashions mainly dependent on the presence or absence of thermal radiation due to solar energy.

1. Introduction

Suspended particulate matter in air, or the atmospheric aerosol, is one of the major ambient air pollution and smog component with natural or anthropogenic sources. Due to the rapid growth of industrialization, urbanization, transportation, deforestation and volcanic eruption, an enormous amount of particles, such as soot and carbon dust emission, is released into the atmosphere in the form of ultrafine aerosol parti-

cles. The nanometer-sized aerosols have considerable effects on health and climate changing. The ultrafine aerosols, with generally larger thermal conductivities than the air, influence the thermal conductivity of the atmospheric environment and affect the earth's energy balance. One of the vital parts of atmospheric aerosols is soot, produced by incomplete combustion of fossil fuel and biomass. Carbon soot has relatively larger thermal conductivity than the pure air, and so has considerable effects on the heat transfer and fluid characteristics of the carrier fluid. However, nanometer-sized particles were added to fluids called nanofluids by Choi [1]. Study of free convection heat transfer

*. Tel.: +98(0)313-7934843; Fax: +98(0)313-7934800
E-mail address: o.ghaffarpasand@gmail.com

of nanofluids in a partitioned cavity has also received significant attention due to its wide engineering applications such as solar collectors, thermal insulation, lubrication technologies, food processing, and cooling of nuclear reactors [2-5]. During recent years, numerous investigations have been conducted on the heat transfer enhancement using nanofluids, considering different utilized numerical methods, various combinations of imposed temperature gradients, and different cavity configurations.

Among the literature published on this subject, Jena & Mahapatra [6] considered the interaction between surface radiation and natural convection of black carbon-air nanofluid in the presence of transverse magnetic field. Results show that increasing the volume fraction of the carbon-black particles causes an enhancement in the heat transfer rate of the atmosphere, which has adverse effect on both climate and living creatures. Mejri et al. [7] treated the effect of magnetic field on the heat transfer and the entropy generation of Al_2O_3-water nanofluid inside an enclosure with sinusoidal heating on both sides of walls. It has been shown that the proper choice of Rayleigh number and solid volume fraction of nanoparticles could be able to maximize heat transfer rate and minimize the entropy generation simultaneously. Mahmoudi et al. [8] investigated numerically the natural convection and entropy generation of Cu-water nanofluid in a trapezoidal enclosure by using the control volume method. They found that the external magnetic field has a tendency to slow down the convection flow within the enclosure. Moumni et al. [9] utilized an accurate finite volume method to study Cu, Ag, Al_2O_3, and TiO_2-water nanofluids in a two-sided lid-driven cavity including discrete heat sources. Results indicate that the nanoparticles with larger thermal conductivity usually cause larger enhancement in heat transfer rate of nanofluid. Chen et al. [10] studied on the entropy generation of double diffusive natural convection of nanofluid in a rectangular enclosure. They found that the total entropy generation is a monotonic decreasing function of nanoparticles volume fraction. Mliki et al. [11] utilized the Lattice Boltzmann Method (LBM) to analyze the buoyancy-driven heat transfer enhancement of the nanofluids in an L-shaped cavity. It has been shown that the presence of high thermal conductive metallic nanoparticles in nanofluids improves the heat transfer and reducing the aspect ratio enhances this effect. Mliki et al. [12] also used the LBM to study natural convection of CuO-water nanofluid in the cavity submitted to different heating modes on its wall in the presence of a uniform heat generation/absorption. Results show that at high Rayleigh numbers, the effect of heat generation or absorption can be ignored. Mahin et al. [13] estimated, both theoretically and experimentally, the values of the

average Nusselt number and heat transfer coefficient ratio for natural convection of silica-water nanofluid in the square or triangular cavities. Kefayati [14] utilized the Finite Difference Lattice Boltzmann Method (FDLBM) to study heat transfer and the entropy generation of non-Newtonian nanofluids in a porous square cavity. His results show that heat transfer and entropy generation increase as Rayleigh number enhances. Shermet et al. [15] performed numerical simulations to study natural convection of nanofluids in an inclined wavy cavity with corner heaters in the presence of a transverse magnetic field. Results indicated that the variation of the cavity inclination angle leads to essential changes in fluid flow and heat transfer. Shermet et al. [16] investigated numerically the entropy generation in natural convection of nanofluid inside a square cavity having hot solid block. The entropy generation due to MHD natural convection of nanofluid inside the entrapped trapezoidal cavities was examined numerically by Selimefendigil et al. [17]. Results show that the magnetic field is more effective in the reduction of the natural convection at the highest value of Rayleigh number.

Most of the atmospheric convection processes deal with the influence of solar energy, thermal radiation, as well as the hydrodynamic partial slip. One of the unsettled questions in the literature is: what is the influence of thermal radiation and hydrodynamic partial slip on the fluid characteristics, heat transfer, and the entropy generation of nanofluids containing ultrafine aerosol particles? Study of the influence of thermal radiation on the natural convection of nanofluids is also important in space technology and high-temperature processes. It plays a considerable role in controlling heat transfer processes and polymer processing industry. On the other hand, there are some important practical situations where partial slip has to be taken into account such as fluoroplastic coating resist adhesion. Meanwhile, partial slips over a moving surface occur for fluids with particulates such as suspensions, emulsions, foams, and polymer solutions. Hence, the answer to this question is also of interest due to wide applications in various fields such as diffusion technology, transpiration cooling, hemodialysis processes, flow control in nuclear reactors, and certain problems of the movement of conductive physiological fluids.

The influence of solar energy radiations on the nanofluid flow over a nonlinearly stretching sheet is addressed by Hady et al. [18]. Zhang et al. [19] analytically studied the flow of nanofluid in the porous medium with variable surface heat flux, chemical reaction, and an external magnetic field. Results indicate that both of magnetic field and radiation greatly affect velocity and temperature fields. Mushtaq et al. [20] investigated the radiation effects due to solar energy

on the stagnation-point flow of nanofluid. They found that the temperature and wall temperature gradient are enhanced with the radiation parameter. Mahmoodi & Kandelousi [21] treated the heat transfer and entropy generation of kerosene-alumina nanofluid in a channel with thermal radiation. Results demonstrate that the Bejan number has a direct relationship with the radiation parameter. Ibáñez et al. [22] utilized the numerical methods to analyze the combined effects of hydrodynamic slip, magnetic field, thermal radiation, nanoparticles volume fraction, and convective boundary conditions on the heat transfer in a viscous electrically conducting nanofluid flow through a microchannel with permeable plates. Bhatti et al. [23] studied numerically the entropy generation with radiation on non-Newtonian Carreau nanofluid towards a shrinking sheet. Results indicate that thermal radiation affects an opposite behavior towards the temperature profile. Sheikholeslami et al. [24] performed numerical simulations to investigate free convection of Al_2O_3-water nanofluid considering thermal radiation in an enclosure with constant flux heating elements. Results show that heat transfer has improved with further enhancement of radiation parameter. Mixed convection of nanofluid in the cavity with partial slip and subjected to a constant heat flux and inclined magnetic field was numerically studied by Ismael et al. [25]. They actually used a constant set of partial slip coefficient during their study, and found that natural convection was decreased with increasing the length of the heat source for all the ranges of the studied parameters. However, there is no open literature available which studies the influence of partial slip or thermal radiation on the entropy generation of nanofluid's convection.

On the other hand, most of the studies reported in the literature have presented their results through the streamlines and isotherms. In fact, streamlines significantly illustrate the fluid flow, whereas isotherms depict only temperature distribution which may not be adequate for the visualization of heat transfer. Heatline visualization is an effective technique to visualize the convective as well as the conductive heat transport in the system. This technique was introduced firstly by Kimura & Bejan [26]. However, although there are enormous studies on natural convection of nanofluids in the literature reporting their results through isotherms, the corresponding research utilizing heatline visualization is sparse. Recently, Basak & Chamkha [27] used the Galerkin finite element method to conduct the heatline analyses on natural convection of nanofluid in a square cavity. Alsabery et al. [28] treated the problem of natural convection in a trapezoidal cavity partly filled with nanofluid by the heatline visualization. Bondareva et al. [29] used this technique to study the natural convection of nanofluid in an inclined wavy open porous cavity. Alsabery et al. [30]

utilized heatline visualization technique to investigate natural convection of nanofluid in a square cavity with sinusoidal temperature variations on both horizontal walls.

However, the study of energy flux through heatlines of natural convection of nanofluid inside the cavity with both of partial slip and thermal radiation has not been undertaken yet. Meanwhile, no proper study is found in the literature which discusses comprehensively the effect of partial slip and thermal radiation on fluid characteristics and heat transfer of nanofluids' natural convection. The present article deals with the investigation of flow field behaviour and heat transfer characteristics of ultrafine aerosol species confined inside the cavity in the presence of thermal radiation due to solar energy and hydrodynamic partial slip. The aerosol is treated as a nanofluid, in which nanometer-sized carbon black particles are suspended in air as the base fluid. A numerical solution is developed to solve the problem, and the effects of embedded parameters are addressed in the current research. Graphical results through the streamlines, isotherms, and heatlines are presented and discussed to deeply understand the physics of the problem. The analysis of entropy generation is also conducted in this study to investigate the effect of pertinent parameters on the various fluid irreversibility cases and demonstrate the thermodynamic optimization of the nanofluid natural convection. This work is very useful in many engineering applications such as metallurgical processes, microelectronics, etc.

2. Mathematical modelling

A sample of ultrafine aerosol spices is enclosed within a two-sided lid-driven square cavity with a side equal to L ($L = 1$), as shown in Figure 1. The vertical
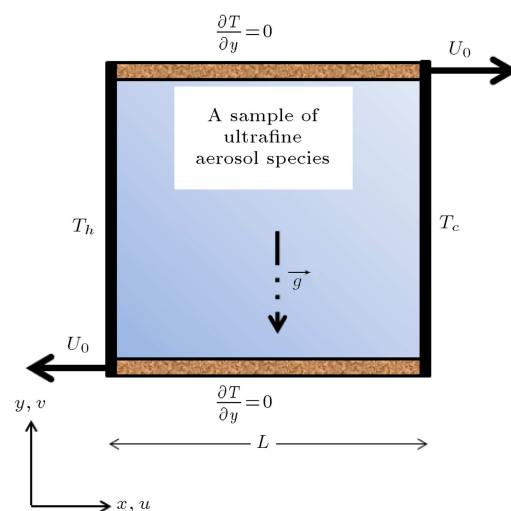

Figure 1. Physical configuration of studied problem and Cartesian coordinates, where $L = 1$.

Table 1. Thermo-physical properties of base fluid and suspended nanoparticles [6].

Physical properties	ρ (kgm^{-3})	C_p (kJkg^{-1}K^{-1})	k (Wm^{-1}K^{-1})	β (K^{-1})
Pure air	1.225	1.005	0.025	3.4×10^{-3}
Carbon-black	2000	0.710	2000	7×10^{-6}

walls have constant temperatures, i.e. T_c and T_h ($T_h > T_c$), while the top and bottom walls are maintained adiabatically and move towards the right and left with constant speed, U_0, respectively. It was assumed that $T_c = 288.5$ K and $T_h = 298.5$ K. The base fluid and suspended nanometer-sized particles are in the thermal equilibrium with each other and no-slip occurs between them. The nanofluid flow is assumed to be incompressible, steady, and laminar in the working range of parameters, and all physical properties except the density in the buoyancy term are assumed to be constant. In other words, the Boussinesq approximation is utilized during this study. Ultrafine carbon particles with fixed diameter of 40 nm are assumed as the suspended aerosols, and the physical properties of the base fluid (pure air with Pr = 0.71) and suspended nanoparticles are provided in Table 1. Joule heating and viscous dissipation are also neglected. Under the above assumptions, the continuity equation, conservation equation of linear momentum, and energy for nanofluid can be obtained as follows:

$$\frac{\partial u}{\partial x} + \frac{\partial v}{\partial y} = 0, \tag{1}$$

$$\frac{\partial(uu)}{\partial x} + \frac{\partial(vu)}{\partial y} = -\frac{1}{\rho_{nf}}\frac{\partial p}{\partial x} + \nu_{nf}\left(\frac{\partial^2 u}{\partial x^2} + \frac{\partial^2 u}{\partial y^2}\right), \tag{2}$$

$$\frac{\partial(uv)}{\partial x} + \frac{\partial(vv)}{\partial y} = -\frac{1}{\rho_{nf}}\frac{\partial p}{\partial y} + \nu_{nf}\left(\frac{\partial^2 v}{\partial x^2} + \frac{\partial^2 v}{\partial y^2}\right)$$

$$+ \frac{(\rho\beta)_{nf}}{\rho_{nf}}g(T - T_c), \tag{3}$$

$$\frac{\partial(uT)}{\partial x} + \frac{\partial(vT)}{\partial y} = \alpha_{nf}\left(\frac{\partial^2 T}{\partial x^2} + \frac{\partial^2 T}{\partial y^2}\right)$$

$$- \frac{1}{(\rho C_P)_{nf}}\left(\frac{\partial q_{rx}}{\partial x} + \frac{\partial q_{ry}}{\partial y}\right), \tag{4}$$

where q_{rx} and q_{ry} are radiative heat fluxes in x and y directions, respectively. According to the Rosseland's approximation, $q_{rx} = -\frac{4\sigma_e}{3\beta_R}\frac{\partial T^4}{\partial x}$ and $q_{ry} = -\frac{4\sigma_e}{3\beta_R}\frac{\partial T^4}{\partial y}$, where σ_e and β_R are Stephan-Boltzmann constant and mean absorption coefficient, respectively. Following Rapits [31], the fluid-phase temperature differences within the flow are assumed to be small enough, whereby temperature variation T^4 may be expanded in a Taylor's series. Neglecting higher order terms yields

$T^4 \simeq 4T_c^3 T - 3T_c^4$, and so:

$$\frac{\partial q_{rx}}{\partial x} = -\frac{16\sigma_e T_c^3}{3k^*}\frac{\partial^2 T}{\partial x^2}, \qquad \frac{\partial q_{ry}}{\partial y} = -\frac{16\sigma_e T_c^3}{3k^*}\frac{\partial^2 T}{\partial y^2}, \tag{5}$$

where k^* is the Rosseland mean absorption coefficient. The effective density at the reference temperature, thermal diffusivity, the heat capacitance, and the thermal expansion coefficient of the nanofluid based on classical models can be written as follows [9]:

$$\rho_{nf} = (1 - \phi)\rho_f + \phi\rho_p, \tag{6}$$

$$\alpha_{nf} = \frac{k_{nf}}{(\rho C_p)_{nf}}, \tag{7}$$

$$(\rho C_p)_{nf} = (1 - \phi)(\rho C_p)_f + \phi(\rho C_P)_p, \tag{8}$$

$$(\rho\beta)_{nf} = (1 - \phi)(\rho\beta)_f + \phi(\rho\beta)_p, \tag{9}$$

where ϕ is the solid volume fraction of the nanoparticles. It is well known that Brownian motion has significant impact on the thermal conductivity of nanofluid containing ultrafine aerosol particles. Koo, Kleinstreuer and Li [32,33] proposed two parts for thermal conductivity of a nanofluid including Brownian motion effects, whereby it can be written as follows:

$$k_{nf} = k_{\text{static}} + k_{\text{Brownian}}, \tag{10}$$

where k_{static} is the static thermal conductivity based on Maxwell-Garnett classical correlation [34] and can be defined as follows:

$$k_{\text{static}} = k_f \frac{k_s + 2k_f - 2\phi(k_f - k_s)}{k_s + 2k_f + \phi(k_f - k_s)}. \tag{11}$$

However, k_{Brownian} is defined by introducing two empirical functions, β and f, whereby they can be written as follows:

$$k_{\text{Brownian}} = 5 \times 10^4 \beta\phi\rho_f C_{Pf}\sqrt{\frac{\kappa_b T}{\rho_p d_p}}f(T, \phi), \tag{12}$$

$$f(T, \phi) = (-6.04\phi + 0.4705)T + (1722.3\phi - 134.63), \tag{13}$$

$$\beta = 0.0137(100\phi)^{-0.8229}, \qquad \text{for} \quad \phi < 1\%, \tag{14}$$

$$\beta = 0.001(100\phi)^{-0.7272}, \qquad \text{for} \quad \phi \geq 1\%. \tag{15}$$

The effective viscosity of nanofluid was also considered according to Koo and Kleinstreuer model [32]. They proposed:

$$\mu_{\text{eff}} = \mu_{\text{static}} + \mu_{\text{Brownian}} = \mu_{\text{static}} + \frac{k_{\text{Brownian}}}{k_f}\frac{\mu_f}{\text{Pr}}, \quad (16)$$

where $\mu_{\text{static}} = \frac{\mu_f}{(1-\phi)^{2.5}}$ is the viscosity of the nanofluid proposed originally by Brinkman [35].

The boundary conditions, including partial slip on horizontal walls, are:

On the left wall:

$$u = v = 0, \qquad T = T_h,$$

On the right wall:

$$u = v = 0, \qquad T = T_c,$$

On the top wall (partial slip):

$$v = 0, \qquad u = \lambda_t U_0 + N\mu_{nf}\frac{\partial u}{\partial y}, \qquad \frac{\partial T}{\partial y} = 0,$$

On the bottom wall (partial slip):

$$v = 0, \qquad u = \lambda_b U_0 + N\mu_{nf}\frac{\partial u}{\partial y}, \qquad \frac{\partial T}{\partial y} = 0.$$

Introducing the following dimensionless variables:

$$(X, Y) = \frac{(x, y)}{L}, \qquad (U, V) = \frac{(u, v)}{U_0},$$

$$\Theta = \frac{T - T_c}{T_h - T_c}, \qquad P = \frac{p}{\rho_{nf}U_0^2}, \quad (17)$$

and using Eqs. (6)-(16), the dimensionless forms of the governing equations are written as follows:

$$\frac{\partial U}{\partial X} + \frac{\partial V}{\partial Y} = 0, \quad (18)$$

$$\frac{\partial}{\partial X}\left(U^2 + \frac{1}{\text{Re}}\left(\frac{\rho_f}{\rho_{nf}}\right)P - \frac{1}{\text{Re}}\left(\frac{\nu_{nf}}{\nu_f}\right)\frac{\partial U}{\partial X}\right)$$
$$+ \frac{\partial}{\partial Y}\left(UV - \frac{1}{\text{Re}}\left(\frac{\nu_{nf}}{\nu_f}\right)\frac{\partial U}{\partial Y}\right) = 0, \quad (19)$$

$$\frac{\partial}{\partial X}\left(UV - \frac{1}{\text{Re}}\left(\frac{\nu_{nf}}{\nu_f}\right)\frac{\partial V}{\partial X}\right)$$
$$- \frac{\partial}{\partial Y}\left(V^2 + \left(\frac{\rho_f}{\rho_{nf}}\right)P - \frac{1}{\text{Re}}\left(\frac{\nu_{nf}}{\nu_f}\right)\frac{\partial V}{\partial Y}\right)$$
$$- \left(\frac{\rho_f}{\rho_{nf}}\right)\left((1-\phi) + \phi\frac{\rho_p\beta_p}{\rho_f\beta_f}\right)\text{Ri}\Theta = 0, \quad (20)$$

$$\frac{\partial}{\partial X}\left(U\Theta - \left(\frac{1}{\text{Re}\,\text{Pr}}\frac{\alpha_{nf}}{\alpha_f} + \frac{4}{3}Rd\left(\frac{k_f}{k_{nf}}\right)\right)\frac{\partial\Theta}{\partial X}\right)$$
$$+ \frac{\partial}{\partial Y}\left(V\Theta - \left(\frac{1}{\text{Re}\,\text{Pr}}\frac{\alpha_{nf}}{\alpha_f} + \frac{4}{3}Rd\left(\frac{k_f}{k_{nf}}\right)\right)\frac{\partial\Theta}{\partial Y}\right)$$
$$= 0. \quad (21)$$

The problem of natural convection is characterized here by the following dimensionless parameters:

$$\text{Ri} = \frac{\text{Gr}}{\text{Re}^2} = \frac{g\beta\Delta T L^3/\nu_f^2}{U_0 L/\nu_f}, \qquad \text{Pr} = \frac{\nu_f}{\alpha_f},$$

$$Rd = \frac{4\sigma_e T_c^3}{\beta_R \kappa_b},$$

where Ri, Gr, Re, Pr, and Rd are Richardson, Grashof, Reynolds, Prandtl numbers, and radiation parameter, respectively. The dimensionless boundary conditions are also given as follows:

On the left wall:

$$U = V = 0, \qquad \Theta = 1, \quad (22)$$

On the right wall:

$$U = V = 0, \qquad \Theta = 0, \quad (23)$$

On the top wall (partial slip):

$$V = 0, \qquad U = \lambda_t + S_t\frac{\mu_{nf}}{\mu_f}\frac{\partial U}{\partial Y}, \qquad \frac{\partial\Theta}{\partial Y} = 0, \quad (24)$$

On the bottom wall (partial slip):

$$V = 0, \qquad U = \lambda_b + S_b\frac{\mu_{nf}}{\mu_f}\frac{\partial U}{\partial Y}, \qquad \frac{\partial\Theta}{\partial Y} = 0, \quad (25)$$

where $S_t = S_b = \frac{N}{L}$. In this study, $S_t = S_b = \lambda$ is called partial slip coefficient and $\lambda_t = -\lambda_b = 1$. The local and average Nusselt numbers of nanofluid along the heated vertical wall can be defined as follows:

$$\text{Nu}_l(Y) = -\left(\frac{k_{nf}}{kf}\right)\left(1 + \frac{4}{3}Rd\left(\frac{k_f}{k_{nf}}\right)\right)\frac{\partial\Theta}{\partial X}|_{Y=0},$$

$$\overline{\text{Nu}} = \int_0^1 \text{Nu}(Y)d.Y. \quad (26)$$

To evaluate the rate of variation due to adding nanoparticles to the nanofluid, the following average Nusselt numbers are defined by imposing partial slip boundary conditions on horizontal walls and applying

thermal radiation:

$$\overline{\mathrm{Nu}}^* = \frac{\overline{\mathrm{Nu}(\phi)} - \overline{\mathrm{Nu}(\text{pure air})}}{\overline{\mathrm{Nu}(\text{pure air})}},$$

$$\overline{\mathrm{Nu}}^\dagger = \frac{\overline{\mathrm{Nu}(\lambda)} - \overline{\mathrm{Nu}(\lambda = 0)}}{\overline{\mathrm{Nu}(\lambda = 0)}},$$

$$\overline{\mathrm{Nu}}^{\dagger\dagger} = \frac{\overline{\mathrm{Nu}(Rd)} - \overline{\mathrm{Nu}(Rd = 0)}}{\overline{\mathrm{Nu}(Rd = 0)}}. \qquad (27)$$

The similar variation rates are also examined and reported for the entropy generation. In this study, the analysis of entropy generation is also conducted. For this purpose, the local entropy generation is defined as follows:

$$S' = S'_F + S'_T$$

$$= \frac{\mu_{nf}}{T_m} \left[2 \left(\frac{\partial u}{\partial x} \right)^2 + 2 \left(\frac{\partial v}{\partial y} \right)^2 + \left(\frac{\partial u}{\partial y} + \frac{\partial v}{\partial x} \right)^2 \right]$$

$$+ \frac{k_{nf}}{T_m^2} \left[\left(\frac{\partial T}{\partial x} \right)^2 + \left(\frac{\partial T}{\partial y} \right)^2 \right]. \qquad (28)$$

The first term of the right-hand side of the above equation represents the local entropy generation due to heat flow, while the second one is due to fluid friction. Using the variables introduced before (Eq. (17)), the dimensionless form of the local entropy generation can be written as follows:

$$S = \frac{k_{nf}}{k_f} \frac{1}{(\Theta + T^*)} \frac{1}{(\Theta + T)^2} \left[\left(\frac{\partial \Theta}{\partial X} \right)^2 + \left(\frac{\partial \Theta}{\partial Y} \right)^2 \right]$$

$$+ \frac{1}{\Theta + T} \frac{\mu_{nf}}{\mu_f} \mathrm{Ec}.\mathrm{Pr} \left[2 \left\{ \left(\frac{\partial U}{\partial X} \right)^2 + \left(\frac{\partial V}{\partial Y} \right)^2 \right\} \right.$$

$$+ \left. \left(\frac{\partial U}{\partial Y} + \frac{\partial V}{\partial X} \right)^2 \right], \qquad (29)$$

where Ec is the local Eckert number, and T^*, S, and Ec are defined as follows:

$$T^* = \frac{T_c k_f}{L}, \qquad S = S' \frac{L^2}{k_f}, \qquad \mathrm{Ec} = \frac{U_0^2}{(C_P)_f \Delta T}. \qquad (30)$$

The contribution of irreversibility due to heat flow in the total entropy generation is usually defined by the Bejan number, which is $\mathrm{Be} = \frac{S_T}{S}$. The average entropy generation and Bejan number are calculated by integrating S and Be in the whole volume occupied by the cavity. In this study, the heat flow pattern is also analyzed through the energy flux vector. The heat

flow within the cavity can be visualized by the heat function, which is the combination of convective and conductive heat fluxes. Following Hooman [36], the scaled heat function H, scaled by $(T_h - T_c)k_f$, is given as follows:

$$\frac{\partial H}{\partial Y} = U\Theta - \left(\frac{1}{\mathrm{RePr}} \frac{\alpha_{nf}}{\alpha_f} + \frac{4}{3} Rd \left(\frac{k_f}{k_{nf}} \right) \right) \frac{\partial \Theta}{\partial X}, \qquad (31)$$

$$-\frac{\partial H}{\partial X} = V\Theta - \left(\frac{1}{\mathrm{RePr}} \frac{\alpha_{nf}}{\alpha_f} + \frac{4}{3} Rd \left(\frac{k_f}{k_{nf}} \right) \right) \frac{\partial \Theta}{\partial Y}. \qquad (32)$$

The first and second terms of the right-hand side of Eqs. (31) & (32) represent, respectively, the convective and conductive heat fluxes along x, y directions. Heat function H satisfies the following Poisson equation:

$$\nabla^2 H = \mathrm{RePr} \frac{(\rho C_P)_{nf}}{(\rho C_P)_f} \left[\frac{\partial(U\Theta)}{\partial Y} - \frac{\partial(V\Theta)}{\partial X} \right]. \qquad (33)$$

The heat function is determined by solving the above Poisson equation subjected to the boundary conditions. It is worthwhile to note that the non-homogenous Dirichlet boundary condition was implied with the heat function.

3. Numerical method, grid in-dependency test, and code validation

The governing equations (Eqs. (18)-(21)) subjected to the boundary conditions (Eqs. (21)-(24)) are solved numerically using an accurate finite volume method. The central difference and the first upwind approaches have been utilized to estimate the diffusive and convective terms, respectively. The resulting discretized equations have been solved using the SIMPLE algorithm [37,38]. In this study, several grid testing cases are performed for different uniform grids, namely, 100×100, 128×128, and 140×140 and for a typical case dealing with $\phi = 0.1$ and Ri = 10. Minor differences of less than 0.3% are detected between produced results by different used grids. Therefore, considering simulated accuracy and CPU time in the range of variables, the uniform grid of 128×128 found enough fine to ensure the grid-independent solution.

The convergence criterion for the termination is also implemented, whereby the following criterion is satisfied for all computations:

$$\max \left| \Gamma_{i,j}^{s+1} - \Gamma_{i,j}^s \right| \leq 10^{-7}, \qquad (34)$$

where s is the iteration number, and Γ stands for the set of U, V, and Θ. Subscript sequence (i, j) denotes the space coordinates of the grid nodes. In order to verify the accuracy of the present methods, the code is validated with the former published results in three

Table 2. Comparison of the average Nusselt numbers for natural convection pure air.

Ra	Hortmann et al. [39]	Ismail & Scalon [40]	Barakos & Mitsoulis [41]	Present study
10^4	2.245	2.256	2.245	2.257
10^5	4.522	4.651	4.510	4.611

Table 3. Comparison of the absolute value of primary vortex, $|\psi_{\max}|$.

Re	Barragy & Carey [42]	Schreiber & Keller [43]	Ismael et al. [44]	Present study
1	0.10005	0.10006	0.10002	0.10006
100	0.10330	0.10330	0.10357	0.10361
400	0.11389	0.11297	0.11212	0.11350
1000	0.11861	0.11603	0.11866	0.11870
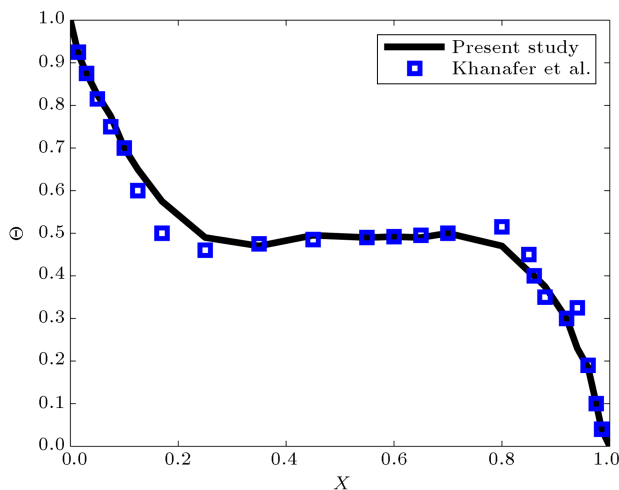
Figure 2. Comparison of the average temperature on the mid plane of the cavity obtained by the present method and results of Khanafer et al. [45], when $Gr = 10^4$ and $\phi = 0.1$.

steps. First, the average Nusselt number for natural convection in the absence of partial slip and thermal radiation was evaluated and compared with the existence benchmark results available in the literature in Table 2. As can be remarked, results obtained from the present method is in good agreement with these results. Then, the absolute value of stream function at primary vortex when $Ri = 10$ was calculated and compared by former published results in Table 3. It should be noted that no-slip boundary conditions were imposed on the walls of the cavity. Acceptable agreement was achieved within the results obtained by various investigators. Furthermore, the variation of average temperature at the mid plane of the cavity for natural convection of Cu-water nanofluid for $Gr = 10^4$ and $\phi = 0.1$ was computed and compared with the results of Khanafer et al. [45] in Figure 2. This comparison shows an acceptable agreement between the results obtained by the present method and those of the previous studies.

4. Results and discussions

The main aim of the current study is the solution to the problem embracing the natural convection of carbon-black solid aerosol particles of the nanometer range suspended in atmospheric air when thermal radiation due to solar energy and hydrodynamic partial slip are all involved. The aerosol is treated as a nanofluid in this study, and Maxwell-Garnetts model accompanied by Koo & Kleinstreuer model for Brownian motion is utilized for estimating the nanofluid viscosity and thermal conductivity. The detailed flow field, temperature distribution, energy flux, and natural convection heat transfer of nanofluid are presented and discussed. The heatline visualization technique is also utilized to study the heat transfer within the cavity in detail. The analysis of entropy generation is also conducted to study the effects of pertinent parameters on the energy loss within the cavity. The studied parameters which pertinently affect the flow and thermal fields inside the studied cavity are: partial slip parameter $\lambda = 1 - 5$, radiation parameter $Rd = 1 - 2$, and solid volume fraction of carbon-black concentration $\phi = 0 - 4\%$. Reynolds number $Re = 100$, Grashof number $Gr = 10^5$, and Prandtl number $Pr = 0.71$ are kept fixed for all computations. According to Richardson number value $Ri = 10$, the flow is dominated by natural convection. Note that the study with the assumed parameter ranges has practical applications in the study of extrusion processes [20] and also many metallurgical processes including the drawing of continuous filaments through quiescent fluids, annealing and tinning of copper wires, etc. [44].

4.1. Effect of hydrodynamic partial slip
To study the effect of partial slip coefficient, zero value is assumed for the radiation parameter during the process. Figures 3(a) to 3(c) present the streamlines, isotherms, and heatlines for different partial slip
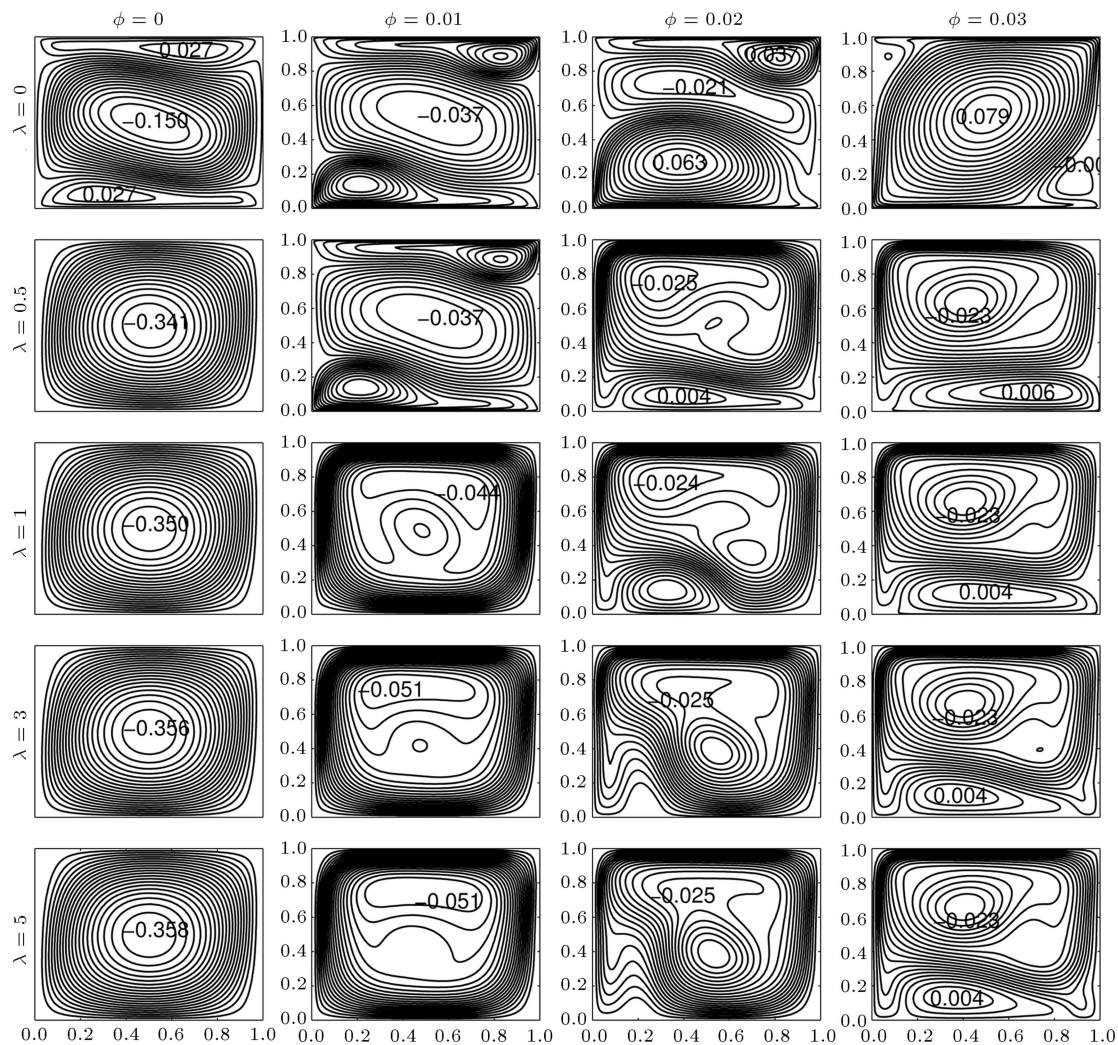
Figure 3a. Streamlines evolution by hydrodynamic partial slip coefficient and solid volume fraction of nanoparticles, when Ri = 10 and $Rd = 0$.

coefficients and various solid volume fractions. For each figure, going from left to right, the solid volume fraction is varied from 0 to 3%, while descending from upper to lower, the partial slip parameter is increased from 0 to 5. However, for $\lambda = 0$, the streamlines are formed into three vortices, a counter-clockwise one in the core of the cavity confined by two clock-wise vortices. The clockwise vortices at the top and bottom half of the cavity are formed by shear forces introduced by moving lids, while the central counter-clockwise vortex is caused by thermal buoyancy forces. In fact, contour level labels designate the direction of the fluid flow and also the strength of the flow.

In the cases of no-slip boundary conditions ($\lambda = 0$), with increasing solid volume fraction of nanoparticles, the counter-clockwise and clockwise vortices are shrunk and expanded, respectively, whereby the whole cavity is occupied by an unicellular clockwise vortex when ϕ is achieved as 3%. Moreover, the stream function values of counter-clockwise and clockwise vortices

are decreased and increased with increasing ϕ value, respectively. It is well known that the inertial forces, viscosity, and thermal conductivity of the nanofluid are enhanced by adding nanoparticles with relatively large density and thermal conductivity. Increasing inertial forces with increasing ϕ leads the cavity to be occupied by a clockwise vortex in cases of large ϕ values, $\phi \geq 3\%$. When the tangential shear stresses at the horizontal boundaries are initiated, λ increases to 0.5, and in cavities filled with pure air $\phi = 0$, the clockwise vortices are disappeared and cavity is occupied by an unicellular counter-clockwise vortex. Moreover, the stream function value of the primary vortex is increased with further enhancement of partial slip coefficient. This fact absolutely shows that the hydrodynamic partial slip eliminates significantly the effect of shear forces. A similar trend has not been observed in the cavities filled with nanofluids, especially at larger values of λ. It can be seen that the influence of hydrodynamic partial slip coefficient on fluid intensity of nanofluids seems to
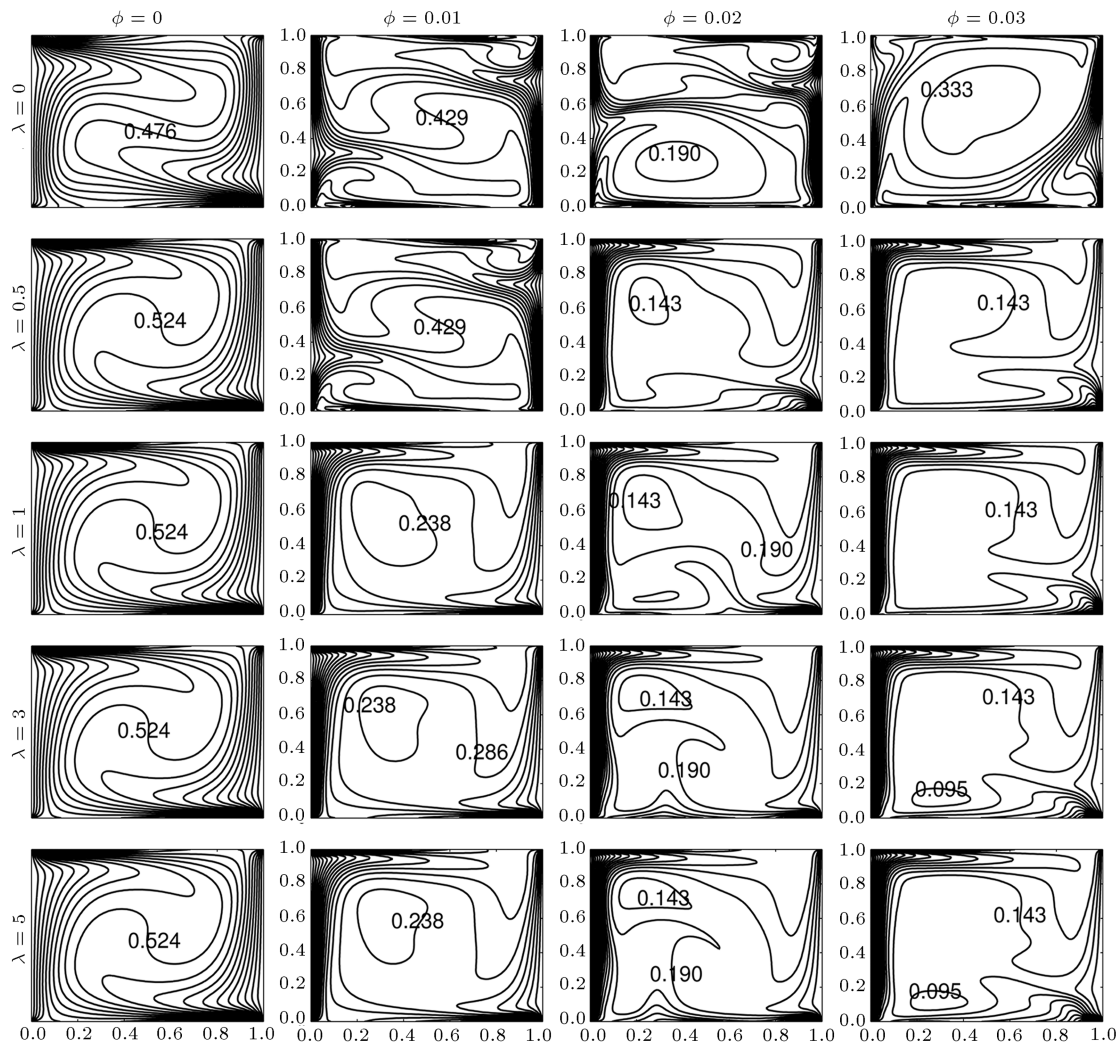
Figure 3b. Isotherms evolution by hydrodynamic partial slip coefficient and solid volume fraction of nanoparticles, when Ri = 10 and $Rd = 0$.

be insignificant. This fact will be also observed further when the variation of the entropy generation due to fluid friction as a function of λ is studied.

The isotherms associated with nanofluid natural convection flow with and without partial slip boundary conditions are shown in Figure 3(b). It can be seen that the concentration of isotherms near the heated wall and the local temperature at the core of the cavity, isotherm line values, are augmented and attenuated by increasing solid volume fraction of nanoparticles, respectively. As observed in Table 1, the ultrafine aerosol particles have relatively larger thermal conductivity than the pure air. This fact has led the convective current of heat across the cavity, which corresponds to the thickness of the thermal boundary layer in vicinity of the heated wall, to improve by adding more volume fraction of nanoparticles. The accumulation of isotherm lines near the heated wall reduces the local temperature at the core of the cavity. However, it seems that the influence of partial slip on isotherms

of cavities filled by pure air is insignificant. When λ is increased to 0.5 in cavities filled with nanofluid, a steep temperature gradient close to the right wall appears, and the central isothermal zone expands to occupy larger part of the cavity with increasing ϕ value. The effect of further enhancement of λ value on temperature distribution seems to be insignificant.

The effects of various values of partial slip coefficients and solid volume fractions of nanoparticles on the heatlines are presented in Figure 3(c). When the natural convection of pure air in cavities with no-slip boundary conditions is considered, $\lambda = \phi = 0$, it can be seen that a singular counter-clockwise heat vortex is confined by two clock-wise heat vortices. The flow of energy through the closed loop indicates the dominance of convective heat transfer. Hence, this figure shows that the energy is transferred across the cavity mainly due to convective current at the core. Increasing partial slip coefficient has an aiding effect on the convective current of energy in cavities filled with
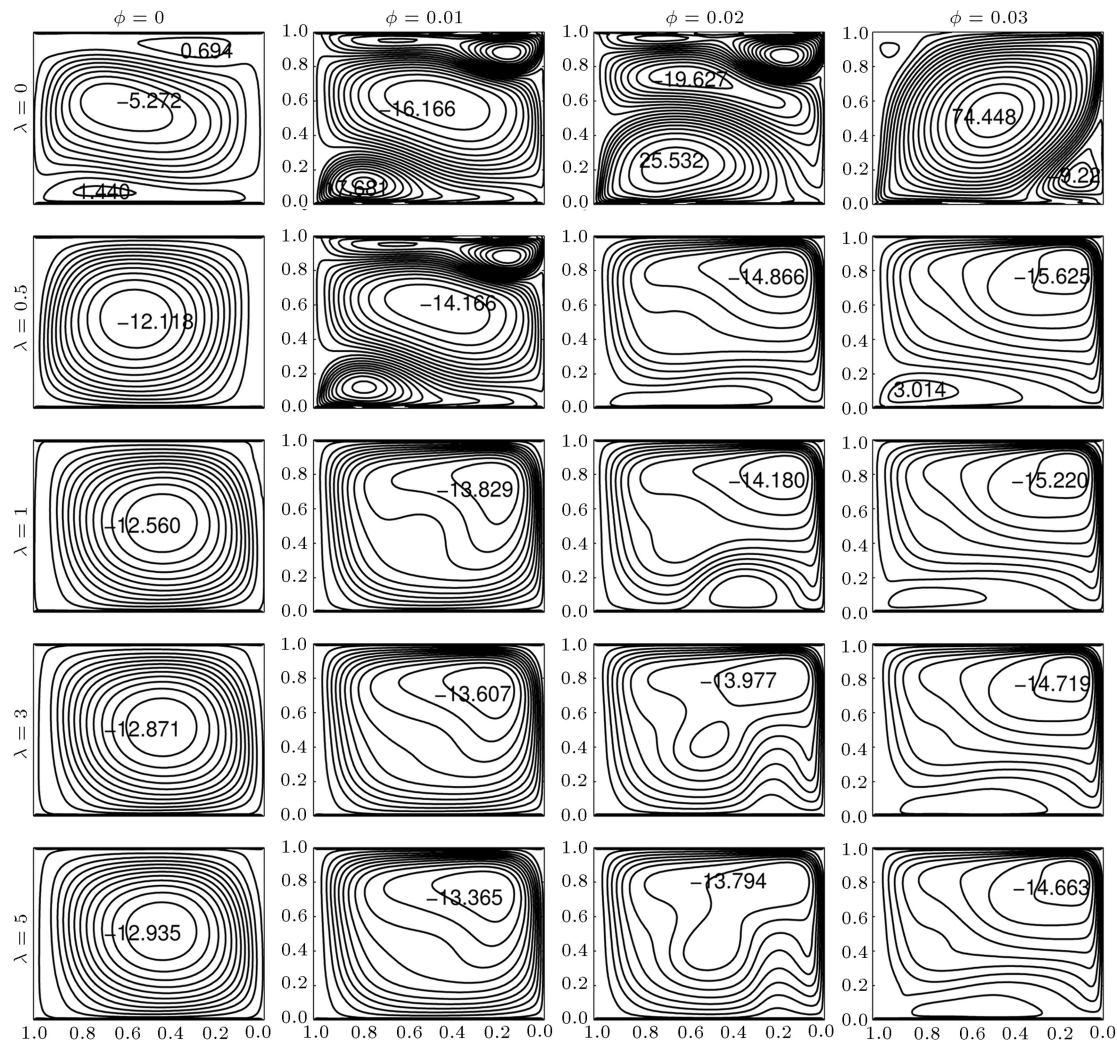
Figure 3c. Heatlines evolution by hydrodynamic partial slip coefficient and solid volume fraction of nanoparticles, when $Ri = 10$ and $Rd = 0$.

pure air, whereby heat function values are increased with increasing λ. In other words, tangential shear stresses imposed by horizontal walls have an opposing action against convective current of heat at the core of the cavity. Moreover, heat function values of nanofluids are enhanced with further enhancement of solid volume fraction of nanoparticles. The existence of nanoparticles with relatively larger thermal conductivity than the pure air improves convective current of heat within the studied enclosure.

In order to evoke careful estimation of what happened along the interesting changes of thermal fields when the partial slip coefficient is varied, average Nusselt number, $\overline{Nu}$, along the heated wall is evaluated and illustrated in Figure 4(a). It can be seen that $\overline{Nu}$ is sharply enhanced when λ changes from zero to 0.5, and then a smooth variation is observed with further increasing of λ value. This result resembles that of Ismael et al. [25] for the cavity filled with pure water. When the partial slip is employed, the lid effect is confused by tangential shear stress along the horizontal walls. In other words, partial slip increases the natural convection across the cavity because it will attenuate the effect of shear forces introduced by moving lids. On the other hand, Figure 4(a) depicts that the average Nusselt number increased with adding more minor volume fraction of nanoparticles, while the opposite is observed when no-slip boundary conditions are imposed. It has been found that the existence of high thermal conductive nanoparticles produces a nanofluid with higher viscosity, higher density, and higher thermal conductivity. The first two properties improve the viscous and inertial forces, while the enhanced thermal conductivity improves the heat transfer. Therefore, the variation of the local Nusselt number shows that the enhanced thermal conductivity dominates both of the enhanced viscous and inertial forces when partial slip is taken into account.

The variation of the average entropy generation as a function of partial slip coefficient is illustrated in

Figure 4(b). First, it can be seen that the average entropy generation enhances with further enhancement of nanoparticles volume fraction. Adding nanoparticles increases the thermal conductivity as well as the viscosity of the nanofluid. This feature causes an enhancement in the irreversibility due to the heat flow and fluid friction, and so it increases the average entropy generation. On the other hand, $\overline{S_{avg}}$ values decrease sharply when λ changes from 0 to 0.5, and then the average entropy generation is insensitive to λ variation. Therefore, it can be concluded that the partial slip has an opposing action against one or all of the fluid irreversibility cases, which will be fairly discussed further.

The variations of the average entropy generation due to fluid friction, $\overline{S_F}$, the contribution of fluid irreversibility due to the heat flow in the total entropy generation, and the average Bejan number are illustrated in Figure 4(c) and (d), respectively. Figure 4(c) elucidates that the influence of solid volume fraction on $\overline{S_F}$ values seems to be insignificant. Nevertheless, it can be seen that the cases with smaller minor volume fraction of nanoparticles have slightly smaller $\overline{S_F}$ values when no-slip boundary conditions are applied. It seems that increasing solid volume fraction of nanoparticles enhances the viscosity of nanofluids, and so improves fluid friction across the cavity with no-slip boundary conditions. However, it can also be seen that applying partial slip boundary conditions to the horizontal walls causes a sharp reduction in the average entropy generation due to fluid friction. Applying partial slip boundary conditions decreases resistance imposed by moving lids and strengths of free convection flow within the cavity. In other words, it reduces the total fluid friction, and so decreases $\overline{S_F}$ value. Meanwhile, after initiation of hydrodynamic partial slip, in cases with $\lambda \neq 0$, the influence of partial slip coefficient on fluid intensity, $\overline{S_F}$, values seems to be insignificant. This feature has been also observed before in Figure 3(a). Figure 4(d) depicts the variation of the average Bejan number as a function of partial slip coefficient for various ϕ values. It is obvious that adding more high thermal conductive solid nanoparticles will generate a nanofluid with a higher thermal conductivity which transfers better thermal energy. Hence, the contribution of irreversibility due to heat flow in the total entropy generation increases with further enhancement of solid volume fraction of
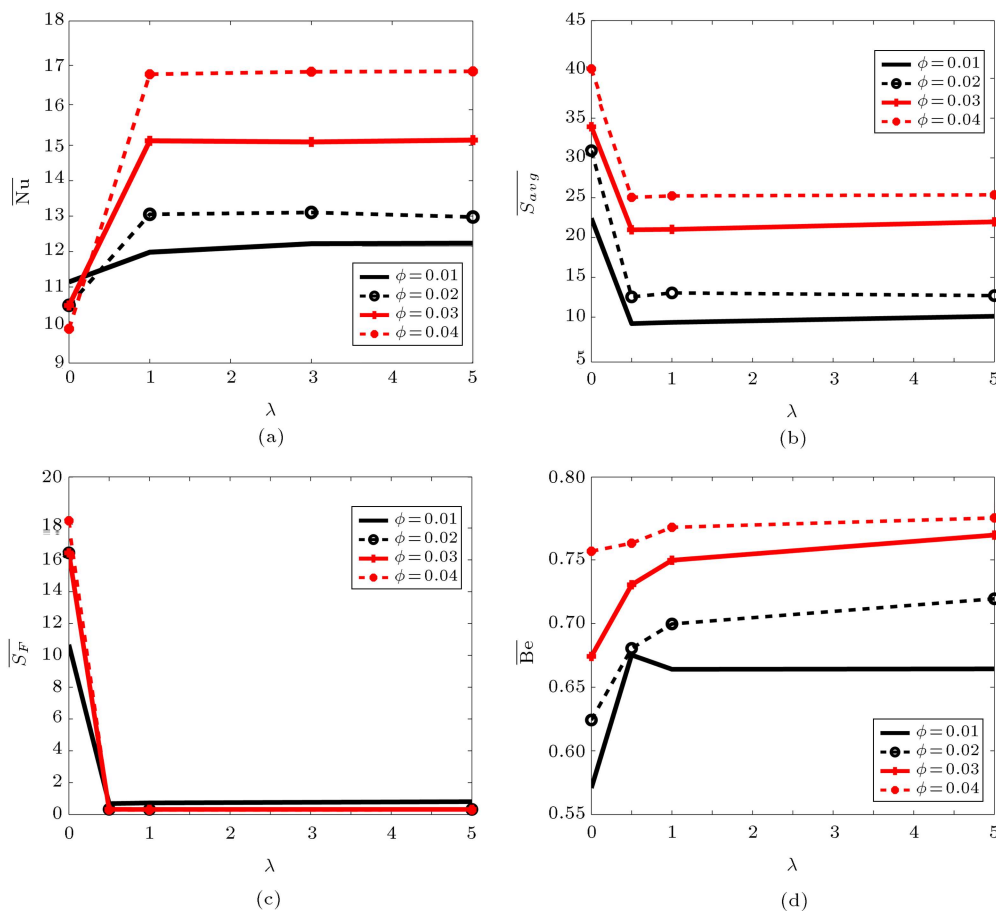

Figure 4. Effects of hydrodynamic partial slip coefficient and solid volume fraction of nanoparticles on the average (a) Nusselt number, (b) entropy generation, (c) entropy generation due to fluid friction, and (d) Bejan number, when Ri = 10 and $Rd = 0$.
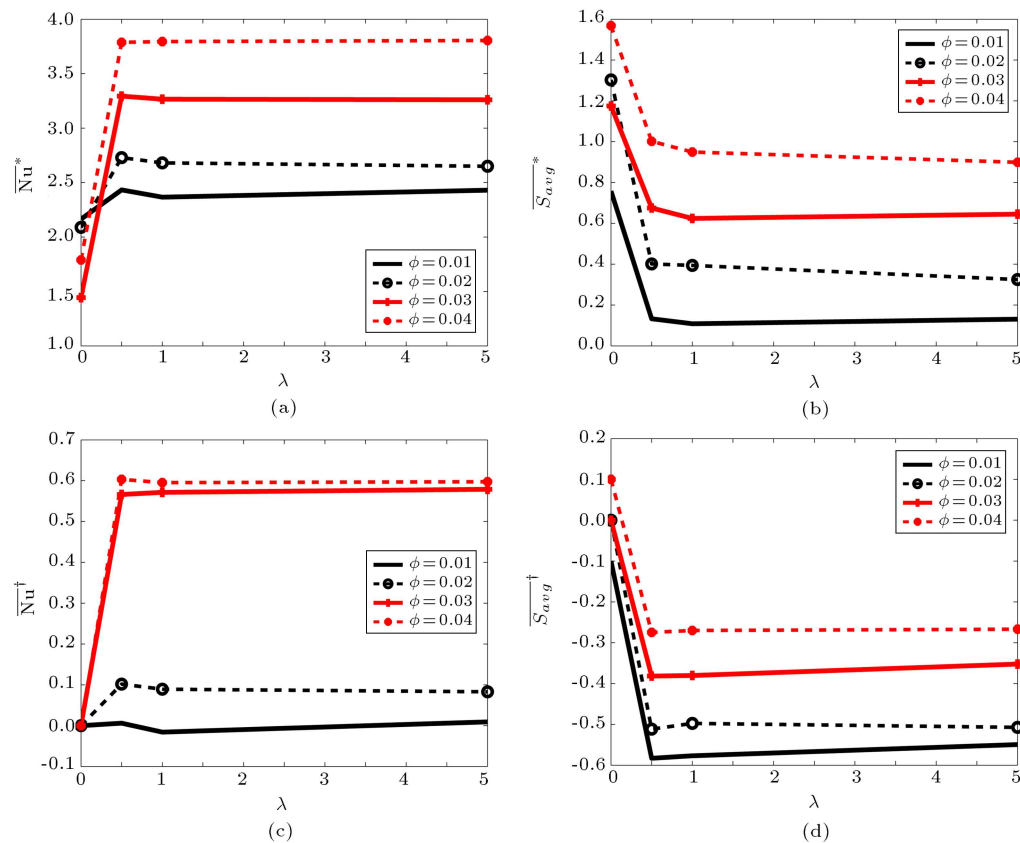
Figure 5. Effects of hydrodynamic partial slip coefficient and solid volume fraction of nanoparticles on the variation in rates of the average (a) Nusselt number and (b) entropy generation due to adding nanoparticles, and the variation in rates of average (c) Nusselt number and (d) entropy generation due to applying partial slip boundary conditions, when Ri = 10 and $Rd = 0$.

nanoparticles. Furthermore, the value of $\overline{Be}$ increases with the increase of partial slip coefficient. It may be noted that with the increase of λ, the shear effect reduces and the buoyancy effect increases for which the irreversibility due to heat transfer increases.

Figure 5 illustrates the variation in rates of the average Nusselt number and entropy generation due to adding minor volume fraction of nanoparticles and applying partial slip boundary conditions. Figure 5(a) elucidates that adding high thermal conductive nanoparticles to the base fluid increases heat transfer, whereby all $\overline{Nu}^*$ values are larger than zero. Meanwhile, after an enhancement of the average Nusselt number due to applied partial slip boundary conditions, $\overline{Nu}^*$ values are insensitive to variation of λ values.

Figure 5(b) shows that the influence of nanoparticles on the average entropy generation is reduced by applying partial slip boundary conditions. Figure 5(c) depicts the effect of solid volume fraction of nanoparticles on the heat transfer enhancement rate due to applied partial slip boundary conditions. It can be seen that $\overline{Nu}^\dagger$ values increase greatly when 2% more nanoparticles are added to the nanofluid. The existence of ultrafine atmospheric aerosols has also developed the entropy generation reduction rate due to applying

partial boundary conditions, whereby $\overline{S_{avg}}^\dagger$ values have been enhanced with further increase of ϕ values. In other words, the ultrafine aerosol particles suspended in the atmosphere improve the heat transfer on one side and develop energy balance on the other.

4.2. Effect of thermal radiation due to solar energy

To reveal the effect of thermal radiation due to solar energy on the natural convection of nanofluid in the presence of partial slip, in this subsection, we set Ri = 10 and $\lambda = 1$, while $0 \le Rd \le 2$. Figure 6 presents streamlines, isotherms, and heatlines, whereby for each figure, going from left to right, the solid volume fraction of nanoparticle ϕ is varied from 0 to 3%, while descending from upper to lower, the radiation parameter increases from 0 to 2. As mentioned and discussed before, the streamlines are usually formed into three vortices, a single counter-clockwise one in the core caused by temperature gradient confined by two clockwise vortices caused by mechanical forces. However, Figure 6(a) shows that the intensity of single counter-clockwise vortex formed by thermal buoyancy forces is augmented with increasing thermal radiation parameter, while the opposite is observed for clockwise vortices. In
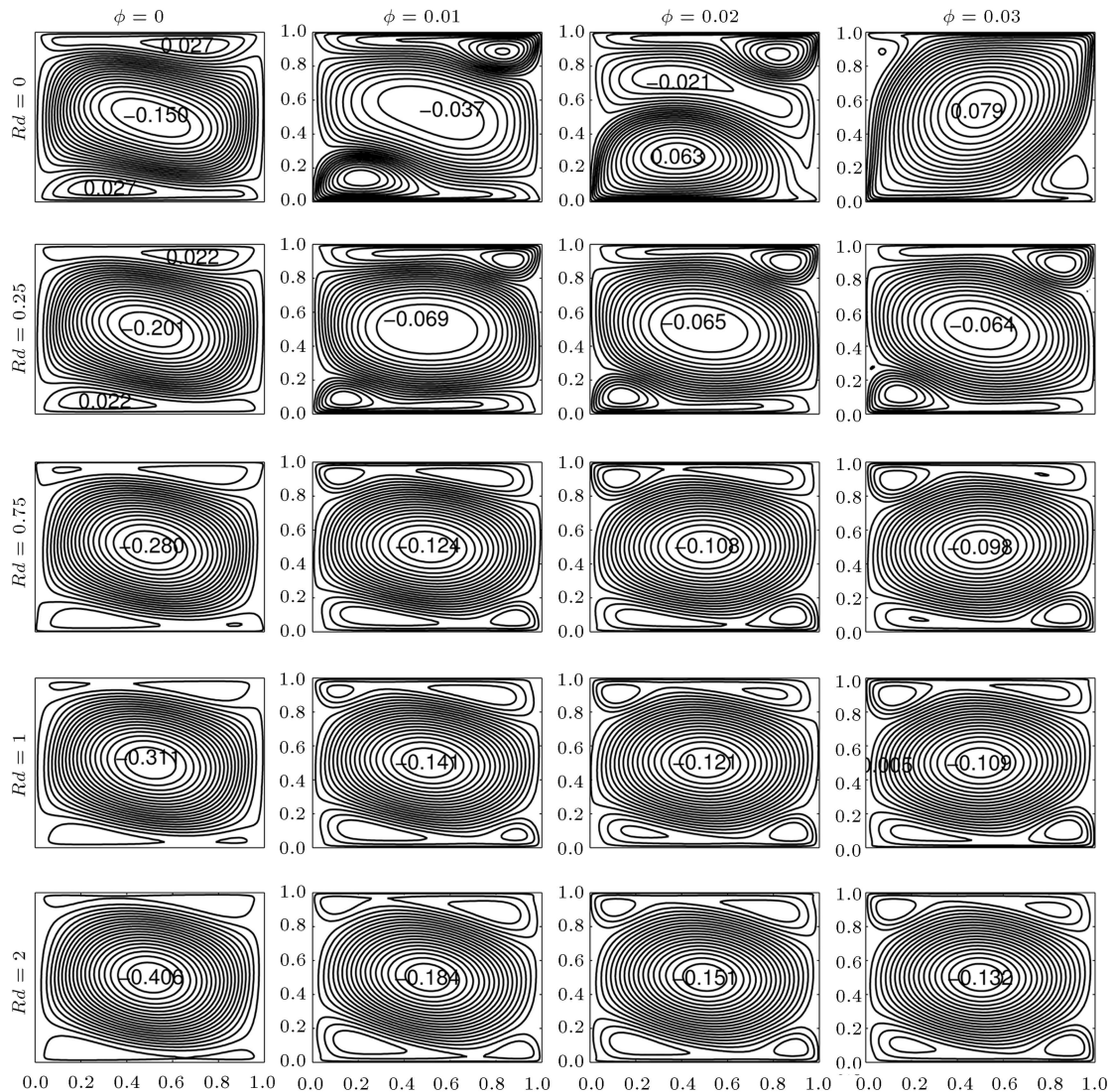
Figure 6a. Streamlines evolution by thermal radiation parameter and solid volume fraction of nanoparticles, when Ri = 10 and $\lambda = 1$.

other words, when Rd is increased, the fluid movement improves due to natural convection and may attenuate the influence of the shear forces due to lids movement. The aiding effect of Rd parameter on the fluid intensity of natural convection has been also observed before in the experimental study of Naghib et al. [46], where the natural convection induced by solar radiation in a water-filled square cavity was investigated. They observed that fluid intensity enhances as the time of solar radiation increases. The time of radiation has a direct relationship with the radiation parameter. This correspondence may be utilized to justify the use of the Rosseland's approximation in the present study.

It can also be seen that the stream function value of the single counter-clockwise vortex occupying the bulk of the cavity was decreased by increasing ϕ values. Adding nanoparticles to the base fluid increases viscosity and fluid friction within the cavity, which

may attenuate the nanofluid movement due to natural convection. The influence of radiation parameter on temperature distribution is illustrated in Figure 6(b). It can be seen that the thickness of thermal boundary layer near the vertical heated walls is reduced with further enhancement of thermal radiation parameter. This can be attributed to the features of thermal radiation which homogenize the medium thermally. The effective driving potential for convection slightly gets reduced at the core in the presence of thermal radiation. This result resembles the results of study of Jena & Mahapatra [6], where the interaction of surface radiation and natural convection of atmospheric aerosol in the presence of transverse magnetic field was studied. However, it can also be observed that the isotherms are no longer orthogonal to the insulated walls as both of the solid volume fraction of nanoparticles and thermal radiation parameter increase simultaneously.
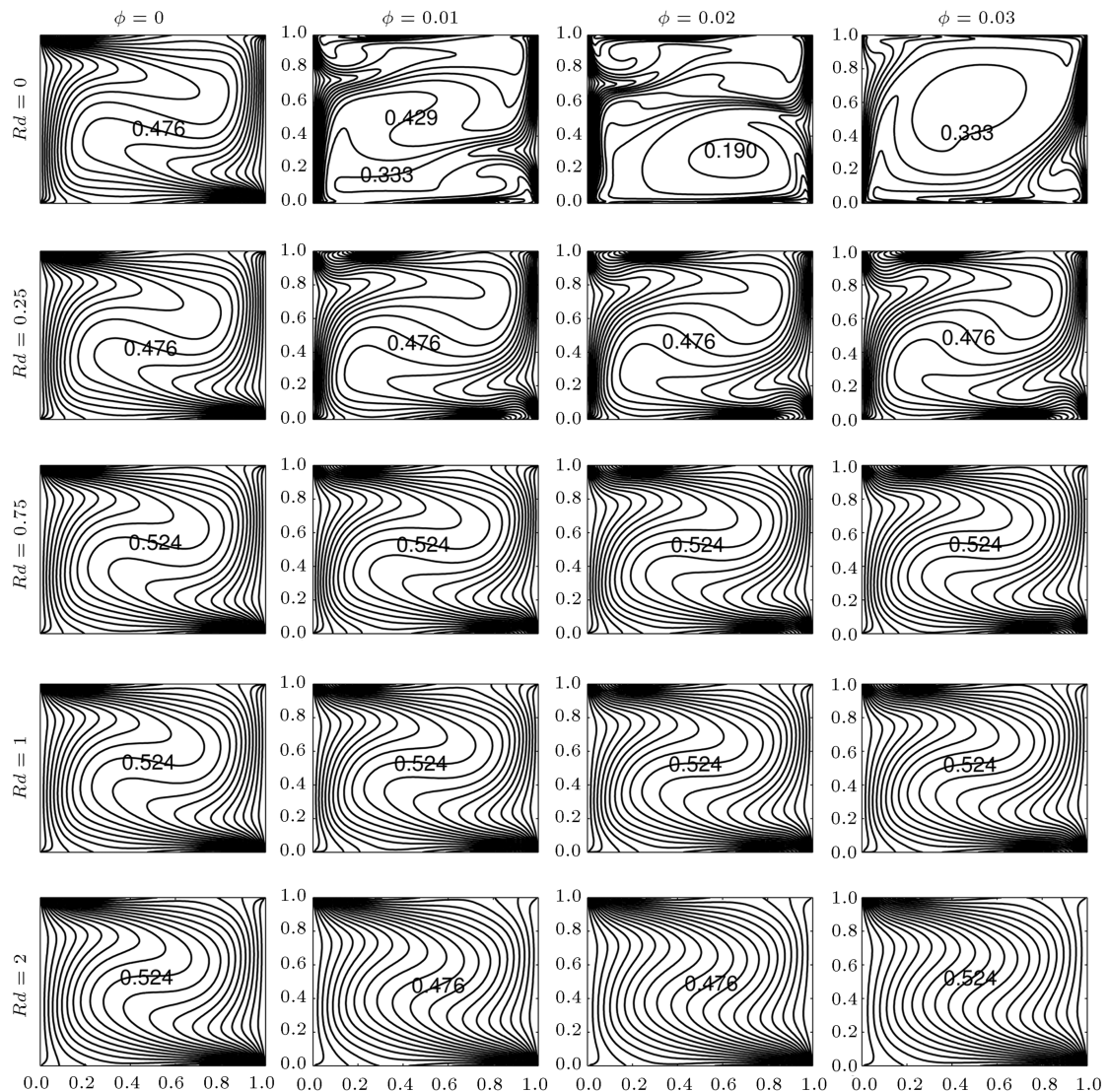
Figure 6b. Isotherms evolution by thermal radiation parameter and solid volume fraction of nanoparticles, when Ri = 10 and $\lambda = 1$.

This feature reveals that the conductive heat transfer enhances and the cavity becomes a quasi-conductive domain as both of Rd and ϕ increase. The influence of thermal radiation due to solar energy as well as the solid volume fraction of nanoparticles on the heatlines is presented in Figure 6(c). This figure elucidates that the value of heat function value for three vortices is augmented by increasing ϕ values for all nan-zero Rd parameters. It means that adding more volume fraction of nanometer-sized aerosol particles in the presence of thermal radiation improves the energy flux across the cavity. On the other hand, it can be seen that the heat function value of single core counter-clockwise vortex is increased with further enhancement of Rd values. This feature indicates that thermal radiation, which homogenizes the medium thermally, facilitates the free convection flow within the core of the enclosure.

Figure 7(a) illustrates the effect of radiation parameter on the average Nusselt number for different solid volume fractions. In the absence of thermal radiation ($Rd = 0$), adding high thermal conductive nanoparticles to the base fluid increases the heat transfer of nanofluid, while the opposite is observed in the cases with $Rd \neq 0$. It seems that the existence of nanoparticles when accompanied by thermal radiation has an opposing action against natural flow within the cavity, whereby $\overline{\text{Nu}}$ is reduced with ϕ in the cases with $Rd \neq 0$. It can also be seen that $\overline{\text{Nu}}$ reduces to a maximum value with increasing Rd to 0.5, and then it increases with further enhancement of radiation parameter. It seems that although the effective driving potential for convection flow at the core reduces with thermal radiation, homogenizing the medium thermally reduces fluid friction to some extent and improves convective current of heat within the
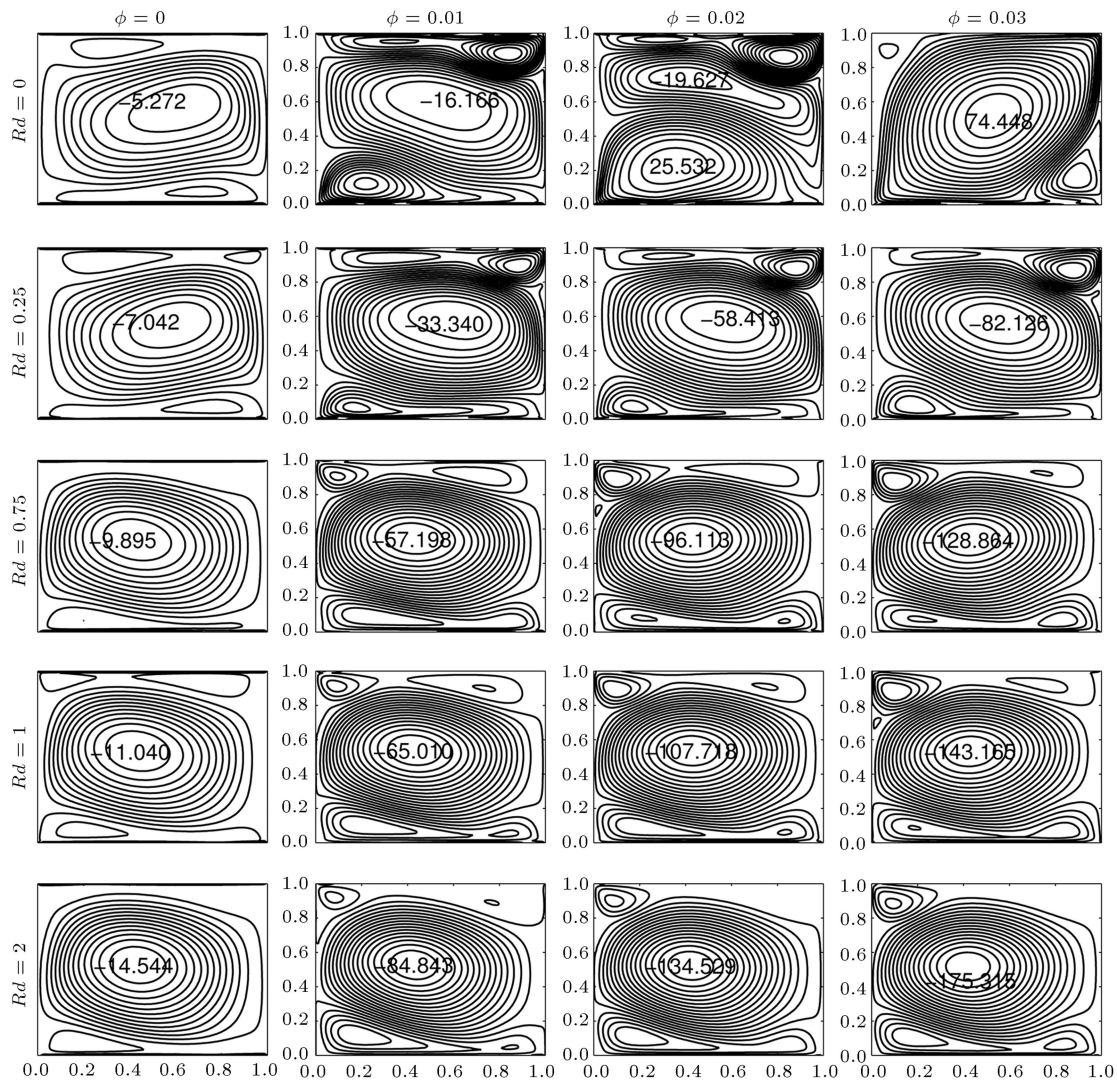
Figure 6c. Heatlines evolution by thermal radiation parameter and solid volume fraction of nanoparticles, when Ri = 10 and $\lambda = 1$.

cavity. This fact has been also observed before in Figure 6(c), where heat function values were enhanced with Rd.

Figure 7(b) elucidates the effect of radiation parameter on the average entropy generation for different solid volume fractions. Increasing radiation parameter reduces the entropy generation. It seems that thermal homogenization caused by increasing thermal radiation reduces the fluid friction and also the other fluid irreversibility cases which result in decreasing the average entropy generation. On the other hand, adding high thermal conductive nanoparticles to the nanofluid in the presence of thermal radiation improves the irreversibility due to heat flow, and so increases the average entropy generation.

The variation of the entropy generation due to fluid friction as a function of thermal radiation coefficient is presented in Figure 7(c). As mentioned before, increasing the radiation parameter homogenizes the medium thermally, which results in decreasing fluid friction within the cavity. Therefore, the entropy generation due to fluid friction reduces with the radiation parameter. In contrast, adding nanoparticles increases viscosity and further fluid friction of nanoparticles, whereby $\overline{S_F}$ is an increasing function of ϕ. The influence of thermal radiation on the average Bejan numbers for different ϕ values is depicted in Figure 7(d). It can be seen that with increasing Rd from zero, $\overline{Be}$ values increase to a maximum value, and then it reduces monotonically with further enhancement of radiation parameter. It seems that increasing thermal radiation parameter, which harmonizes the medium thermally, has an aiding effect on natural flow of nanofluid, and so has an opposing action on conductive heat transfer. On the other hand, as observed in Figure 7(c), applying thermal radiation causes a reduction in fluid friction irreversibility which results in increasing Bejan number. The irreversibility due to heat flow has a direct

relationship with the conductive heat transfer (see Eq. (27)). However, increasing solid volume fraction of nanoparticles when accompanied by thermal radiation increases the conductive mode of heat transfer, and so the contribution of irreversibility due to thermal effects on the total entropy generation ($\overline{Be}$) improves with increasing ϕ value.

The variations in rates of the average Nusselt number and entropy generation due to adding ultrafine aerosol particles to the pure air as a function of radiation parameter are illustrated in Figure 8(a) and (b), respectively. It can be seen that both of them are a reduction function of radiation parameter. Adding high thermal conductive nanoparticles in the presence of thermal radiation improves the conductive mode of heat transfer across the cavity. Therefore, it can be claimed that thermal radiation has an opposite action on the heat transfer enhancement due to adding nanoparticles. On the other hand, increasing thermal radiation reduces fluid friction across the cavity, and so has also an opposite action on the entropy generation enhancement due to adding nanoparticles. It is obvious that the fluid friction as well as the irreversibility due to thermal effects on nanofluids with larger solid volume fraction of nanoparticles are higher than the others.

The variations in rates of average Nusselt number and the entropy generation due to applying thermal radiation are depicted in Figure 8(c) and (d), respectively. First, it is obvious that thermal radiation causes a reduction in both of $\overline{Nu}$ and $\overline{S_{avg}}$, whereby all values of those figures are negative. Nevertheless, it seems that $\overline{Nu}^{\dagger\dagger}$ values reduce to a minimum value with increasing Rd from 0 to 0.5, and then increases monotonically with further enhancement of thermal radiation parameter. Nanofluids with larger solid volume fractions are affected greatly by thermal radiation due to larger negative values of $\overline{Nu}^{\dagger\dagger}$. Besides, the cases with larger ϕ values have larger $\overline{S_{avg}}^{\dagger\dagger}$ values.

5. Summary and conclusions

In this study, steady laminar natural convection of atmospheric aerosol sample enclosed within a two-sided lid-driven cavity in the presence of hydrodynamic partial slip and thermal radiation effects was studied numerically. An accurate finite volume method based on SIMPLE algorithm was adapted, validated, and utilized to solve the governing equations. The Brownian motion effect of nanoparticles was considered by using Koo-Kleinstreuer-Li model for effective thermal conductivity and viscosity of nanofluid. The analysis
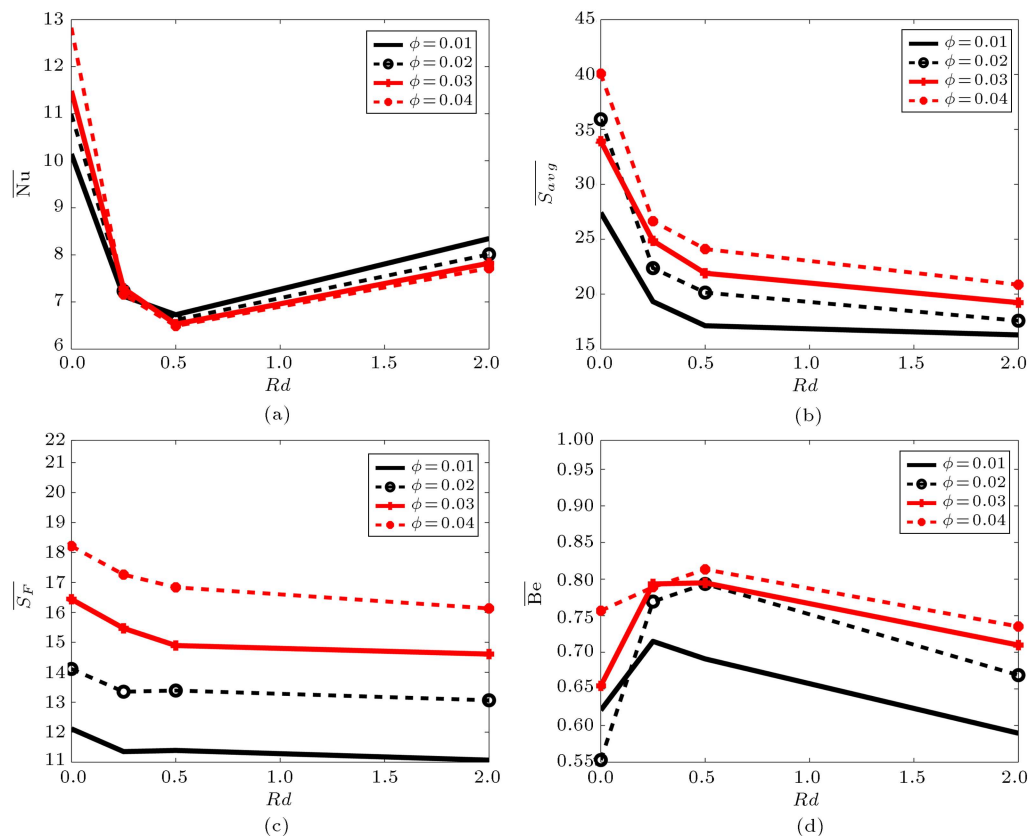

Figure 7. Effects of thermal radiation parameter and solid volume fraction of nanoparticles on the average (a) Nusselt number, (b) entropy generation, (c) entropy generation due to fluid friction, and (d) Bejan number, when Ri = 10 and $\lambda = 1$.
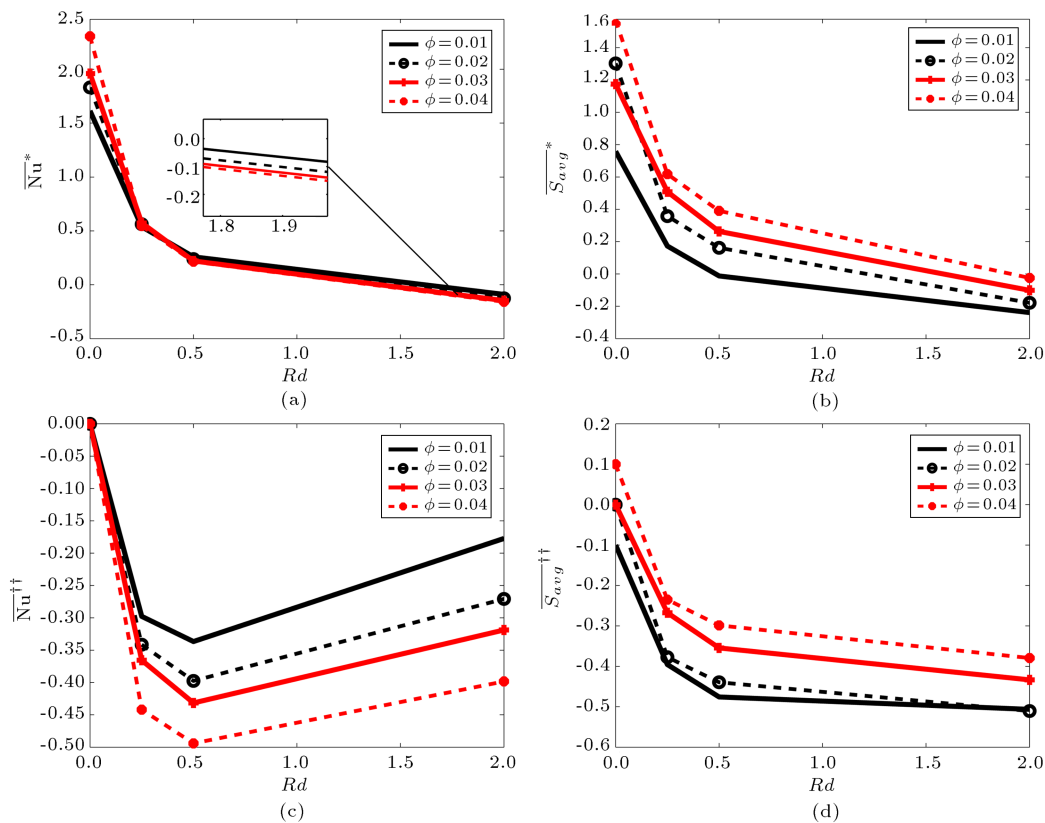
Figure 8. Effects of thermal radiation parameter and solid volume fraction of nanoparticles on the variation in rates of the average (a) Nusselt number and (b) entropy generation due to adding nanoparticles; variation in rates of the average (c) Nusselt number and (d) entropy generation due to imposing thermal radiation.

of entropy generation was conducted and heatline visualization technique was also utilized to study the energy flux within the cavity in more detail. The studied relevant parameters were hydrodynamic partial slip coefficient, thermal radiation parameter, and solid volume fraction of nanoparticles. In view of the above study, the following conclusions are outlined:

1. Partial slip significantly eliminates the effect of shear forces (lid-driven effect), whereby heat function is an increasing function of λ value regardless of solid volume fraction of nanoparticles of nanofluid. Moreover, the average Nusselt number is sharply increased when partial slip is initiated, and then it becomes insensitive to λ variation;

2. Tangential shear stresses imposed by moving lids cause an enhancement and a reduction in fluid irreversibility due to heat flow and fluid friction, respectively, while it usually reduces the total entropy generation;

3. In the absence of thermal radiation, with an increase of solid volume fraction of nanoparticles, both of the heat transfer and entropy generation, regardless of the selected non-zero value of λ, are increased. The presence of nanoparticles usually enhances the thermal conductivity of the nanofluid;

4. Thermal radiation due to solar energy usually homogenizes the temperature distribution. This homogenization reduces fluid friction as well as the average entropy generation;

5. The presence of nanoparticles in nanofluids when accompanied by thermal radiation has an opposing and aiding action on the conductive and convective modes of heat transfer, respectively. This brings about the fact that in cases with $Rd \neq 0$, $\overline{Nu}$ and $\overline{Be}$ are the decreasing and increasing functions of ϕ values, respectively.

Acknowledgments

Nomenclature

d_p	Diameter of particle (nm)
g	Acceleration due to gravity (ms^{-2})
Gr	Grashof number
L	Length of outer cavity (m)

N	Slip constant $(\mathrm{m^2skg^{-1}})$
Nu	Nusselt number
P	Non-dimensional fluid pressure
p	Fluid pressure $(\mathrm{Nm^{-2}})$
p_0	Pressure scale
Pr	Prandtl number
q_r	Radiation heat flux $(\mathrm{Wm^{-2}})$
Re	Reynolds number
Ri	Richardson number
S	Entropy $(\mathrm{JK^{-1}})$
T	Fluid temperature (K)
T_0	Characteristic fluid temperature
U, V	Non-dimensional velocity components
u, v	Velocity components $(\mathrm{ms^{-1}})$
U_0	Absolute lid velocity $(\mathrm{ms^{-1}})$
X, Y	Non-dimensional Cartesian coordinate
x, y	Cartesian coordinate (m)

Greek

α	Thermal diffusivity $(\mathrm{m^2s})$
β_T	Thermal expansion coefficient $(\mathrm{K^{-1}})$
κ_b	Boltzmann constant $(\mathrm{JK^{-1}})$
λ	Dimensionless partial slip parameter
ν	Kinematic viscosity of fluid $(\mathrm{m^2s^{-1}})$
ρ	Fluid density $(\mathrm{kgm^{-3}})$
ρ_0	Characteristic fluid density
σ_e	Stephan-Boltzmann constant
Θ	Dimensionless fluid temperature

Superscript

F	Fluid friction irreversibility
f	Pure fluid
h	High temperature
l	Low temperature
nf	Nanofluid
p	Aerosol particle
T	Heat transfer irreversibility

References

1. Choi, S.U.S. "Enhancing thermal conductivity of fluid with nanoparticles", *ASME Fluid Eng. Div.*, **23**, pp. 99-105 (1995).

2. Khorasanizadeh, H., Amani, J. and Nikfar, M. "Numerical investigation of Cu-water nanofluid natural convection and entropy generation within a cavity with an embedded conductive baffle", *Scientia Iranica F*, **19**, pp. 1996-2003 (2012).

3. Hakeem, A.K.A., Ganesh, N.V. and Ganga, B. "Heat transfer of non-Darcy MHD flow of nanofluid over a stretching/shrinking surface in a thermally stratified medium with second order slip model", *Scientia Iranica F*, **22**, pp. 2766-2784 (2015).

4. Bettaibi, S., Kuznik, F. and Sediki, E. "Hybrid LBM-MRT model coupled with finite difference method for double-diffusive mixed convection in rectangular enclosure with insulated moving lid", *Physica A: Statistical Mechanics and Its Applications*, **444**, pp. 311-326 (2016).

5. Wang, L., Shi, B., Chai, Z. and Yang, X. "Regularized lattice Boltzmann model for double-diffusive convection in vertical enclosures with heating and salting from below", *Appl. Thermal Eng.*, **103**, pp. 365-376 (2016).

6. Jena, S.K. and Mahapatra, S.K. "Numerical modeling of interaction between surface radiation and natural convection of atmospheric aerosol in presence of transverse magnetic field", *J. Appl. Math. Model.*, **37**, pp. 527-539 (2013).

7. Mejri, I. and Mahmoudi, A. "MHD natural convection in a nanofluid-filled open enclosure with a sinusoidal boundary condition", *Chem. Eng. Res. Des.*, **98**, pp. 1-16 (2015).

8. Mahmoudi, A.H., Pop, I., Shahi, M. and Talebi, F. "MHD natural convection and entropy generation in a trapezoidal enclosure using Cu-water nanofluid", *Comput. Fluids*, **72**, pp. 46-62 (2013).

9. Moumni, H., Welhezi, H., Djebali, R. and Sediki, E. "Accurate finite volume investigation of nanofluid mixed convection in two-sided lid-driven cavity including discrete sources", *Appl. Math. Model.*, **39**, pp. 4164-4179 (2015).

10. Chen, Sh., Xiao, X. and Zheng, Ch. "Analysis of entropy generation in double-diffusive natural convection of nanofluid", *Int. J. Heat Mass Transfer*, **87**, pp. 447-463 (2016).

11. Mliki, B., Abbassi, M.A., Omri, A. and Belkacem, Z. "Augmentation of natural convective heat transfer in linearly heated cavity by utilizing nanofluids in the presence of magnetic field and uniform heat generation/absorption", *Powder Technol.*, **284**, pp. 312-325 (2015).

12. Mliki, B., Abbassi, M.A., Omri, A. and Zeghmati, B. "Effects of nanoparticles Brownian motion in a linearly/sinusoidally heated cavity with MHD natural convection in the presence of uniform heat generation/absorption", *Powder Technol.*, **295**, pp. 69-83 (2016).

13. Mahin, O., Kianifar, A., Heris, S.Z. and Wongwises, S. "Natural convection of silica nanofluids in square and triangular enclosures: Theoretical and experimental study", *Int. J. Heat Mass Transfer*, **99**, pp. 792-804 (2016).

14. Kefayati, Gh.R. "Heat transfer and entropy generation of natural convection on non-Newtonian nanofluids in a porous cavity", *Powder Technol.*, **299**, pp. 127-149 (2016).

15. Shermet, M.A., Oztop, H.F. and Pop, I. "MHD natural convection in an inclined wavy cavity with corner heater filled with a nanofluid", *J. Mag. Mag. Mat.*, **416**, pp. 37-47 (2016).

16. Shermet, M.A., Oztop, H.F., Pop, I. and Abu-Hamdeh, N. "Analysis of entropy generation in natural convection of nanofluid inside a square cavity having hot solid block: Tiwari and Das model", *Entropy*, **18**, pp. 9-24 (2016).

17. Selimefendigil, F., Oztop, H.F. and Abu-Hamdeh, N. "Natural convection and entropy generation in nanofluid filled entrapped trapezoidal cavities under the influence of magnetic field", *Entropy*, **18**, pp. 43-65 (2016).

18. Hady, F.M., Ibrahim, F.S., Gaied, S.M.A. and Eid, M.R. "Radiation effect on viscous flow of a nanofluid and heat transfer over a nonlinearly stretching sheet", *Nanoscale Res. Lett.*, **7**, pp. 229-242 (2012).

19. Zhang, C., Zheng, L., Zhang, C. and Chen, G. "MHD flow and radiation heat transfer of nanofluids in porous media with variable surface heat flux and chemical reaction", *Appl. Math. Model.*, **39**, pp. 165-181 (2015).

20. Mushtaq, A., Mustafa, M., Hayat, T. and Alsaedi, A. "Nonlinear radiative heat transfer in the flow of nanofluid due to solar energy: A numerical study", *J. Taiwan Ins. Chem. Eng.*, **45**, pp. 1176-1183 (2014).

21. Mahmoodi, M. and Kandelousi, S. "Effects of thermophoresis and Brownian motion on nanofluid heat transfer and entropy generation", *J. Mol. Liquids*, **211**, pp. 15-24 (2015).

22. Ibáñez, G., López, A., Pantoja, J. and Moreira, J. "Entropy generation analysis of a nanofluid flow in MHD porous microchannel with hydrodynamic slip and thermal radiation", *Int. J. Heat Mass Transfer*, **100**, pp. 89-97 (2016).

23. Bhatti, M.M., Abbas, T., Rashidi, M.M. and Ali, M.El-Sayed "Numerical simulation of entropy generation with thermal radiation on MHD Carreau nanouid towards a shrinking sheet", *Entropy*, **18**, pp. 200-214 (2016).

24. Sheikholeslami, M., Hayat, T. and Alsaedi, A. "MHD free convection of Al_2O_3-water nanofluid considering thermal radiation: A numerical study", *Int. J. Heat Mass Transfer*, **96**, pp. 513-524 (2016).

25. Ismael, M.A., Mansour, M.A., Chamkha, A.J. and Rashad, A.M. "Mixed convection in a nanofluid filled-cavity with partial slip subjected to constant heat flux and inclined magnetic field", *J. Mag. Mag. Mat.*, **416**, pp. 25-36 (2016).

26. Kimura, S. and Bejan, A. "The heatline visualization of convective heat transfer", *J. Heat Transfer*, **105**, pp. 916-919 (1983).

27. Basak, T. and Chamkha, A.J. "Heatline analysis on natural convection for nanofluids confined with square cavities with various thermal boundary conditions", *Int. J. Heat Mass Transfer*, **55**, pp. 5526-5543 (2012).

28. Alsabery, A.I., Chamkha, A.J., Hussain, S.H., Saleh, H. and Hashim, I. "Heatline visualization of natural convection in a trapezoidal cavity partly filled with nanofluid porous layer and partly with non-Newtonian fluid layer", *Adv. Powder Technol.*, **26**, pp. 1230-1244 (2015).

29. Bondareva, N.S., Shermet, M.A., Oztop, H.F. and Abu-Hamdeh, N. "Heatline visualization of MHD natural convection in an inclined wavy open porous cavity filled with a nanofluid with a local heater", *Int. J. Heat Mass Transfer*, **99**, pp. 872-881 (2016).

30. Alsabery, A.I., Chamkha, A.J., Hussain, S.H., Saleh, H. and Hashim, I. "Heatline visualization of conjugate natural convection in a square cavity filled with nanofluid with sinusoidal temperature variations on both horizontal walls", *Int. J. Heat Mass Transfer*, **100**, pp. 835-850 (2016).

31. Rapits, A. "Radiation and free convection flow through a porous medium", *Int. Commun. Heat Mass Transfer*, **25**, pp. 289-295 (1998).

32. Koo, J. and Kleinsstreuer, C. "Viscous dissipation effects in micro tubes and micro channels", *Int. J. Heat Mass Transfer*, **47**, pp. 3159-3169 (2004).

33. Li, J. "Computational analysis of nanofluid flow in micro channels with applications to micro-heat sinks and bio-MEMS", Ph.D. Thesis, NC State University, Raleigh, NC, the United States (2008).

34. Maxwell, J.C., *A Treatise on Electricity and Magnetism*, **II**, Oxford University Press, Cambridge, UK (1983).

35. Brinkman, H.C. "The viscosity of concentrated suspensions and solutions", *J. Chem. Phys.*, **20**, pp. 571-581 (1952).

36. Hooman, K. "Energy flux vector as new tool for convection visualization", *Int. J. Num. Method Heat Fluid Flow*, **20**, pp. 240-249 (2010).

37. Patankar, S.V., *Numerical Heat Transfer and Fluid Flow*, Hemisphere, Washington D.C. (1980).

38. Ghaffarpasand, O. "Effect of alternating magnetic field on unsteady MHD mixed convection and entropy generation of ferrofluid in a linearly heated two-sided cavity", *Scientia Iranica* (2017). Accepted, Available On-line (No. 1931).

39. Hortmann, M., Peric, M. and Scheuener, G. "Finite volume multigrid prediction of laminar natural convection: bench-mark solutions", *Int. J. Num. Methods Fluids.*, **11**, pp. 189-207 (1990).

40. Ismail, K.A.R. and Scalon, V.L. "A finite element free convection model the side wall heated cavity", *Int. J. Num. Methods Fluids.*, **43**, pp. 1373-1389 (1990).

41. Barakos, G. and Mitsoulis, E. "Natural convection flow in a square cavity revisited: laminar and turbulent

models", *Int. J. Num. Methods Fluids.*, **18**, pp. 695-719 (1994).

42. Barragy, E. and Carey, G.F. "Stream function-vorticity driven cavity solution using finite elements", *Comput. Fluids.*, **26**, pp. 453-468 (1997).

43. Schreiber, R. and Keller, H.B. "Driven cavity flows by efficient numerical techniques", *J. Comut. Phys.*, **49**, pp. 310-333 (1983).

44. Ismael, M.A., Pop, I. and Chamkha, A.J. "Mixed convection in a lid-driven square cavity with partial slip", *Int. J. Therm. Sci.*, **82**, pp. 47-61 (2014).

45. Khanafer, K., Vafai, K. and Lightstone, M., "Buoyancy-driven heat transfer enhancement in a two-dimensional enclosure utilizing nanofluids", *Int. J. Heat Mass Transfer*, **19**, pp. 3639-3653 (2003).

46. Naghib, A., Patterson, J.C., Lei, Ch. and Hattori, T. "Natural convection induced by radiation in a water filled square cavity: Experimental observations", *Exp. Therm. Fluid Sci.*, **80**, pp. 105-116 (2017).

Biography

Omid Ghaffarpasand received his PhD from the Department of Physics, University of Isfahan, Iran in 2012. Currently, he is a full-time Faculty Member of Department of Physics, University of Isfahan, Iran. His current research fields include Computational Fluid Dynamics (CFD), aerosol technology, aerosol propagation and deposition mechanisms, aerosol sizing techniques, heat and mass transfer, and magnetohydrodynamic convection in various regimes.